



Full-Scale Crustal Interpretation of Kokkola–Kymi (KOKKY) Seismic Profile, Fennoscandian Shield

TIMO TIIRA,¹ TOMASZ JANIK,² TYMON SKRZYNIK,² KARI KOMMINAHO,¹ AKU HEINONEN,¹ TONI VEIKKOLAINEN,¹ SAKARI VÄKEVÄ,¹ and ANNAKAISA KORJA¹

Abstract—The Kokkola–Kymi Deep Seismic Sounding profile crosses the Fennoscandian Shield in northwest-southeast (NW–SE) direction from Bothnian belt to Wiborg rapakivi batholith through Central Finland granitoid complex (CFGC). The 490-km refraction seismic line is perpendicular to the orogenic strike in Central Finland and entirely based on data from quarry blasts and road construction sites in years 2012 and 2013. The campaign resulted in 63 usable seismic record sections. The average perpendicular distance between these and the profile was 14 km. Tomographic velocity models were computed with JIVE3D program. The velocity fields of the tomographic models were used as starting points in the ray tracing modelling. Based on collected seismic sections a layer-cake model was prepared with the ray tracing package SEIS83. Along the profile, upper crust has an average thickness of 22 km average, and P-wave velocities (V_p) of 5.9–6.2 km/s near the surface, increasing downward to 6.25–6.40 km/s. The thickness of middle crust is 14 km below CFGC, 20 km in SE and 25 km in NW, but V_p ranges from 6.6 to 6.9 km/s in all parts. Lower crust has V_p values of 7.35–7.4 km/s and lithospheric mantle 8.2–8.25 km/s. Moho depth is 54 km in NW part, 63 km in the middle and 43 km in SW, yet a 55-km long section in the middle does not reveal an obvious Moho reflection. S-wave velocities vary from 3.4 km/s near the surface to 4.85 km/s in upper mantle, consistently with P-wave velocity variations. Results confirm the previously assumed high-velocity lower crust and depression of Moho in central Finland.

Keywords: Seismology, reflection, tomography, Moho, Fennoscandia, Precambrian.

1. Introduction

The Precambrian nucleus of Europe, the Fennoscandian Shield (Fig. 1), has been well studied for its deep structure (Grad et al. 2009) with long-ranging DSS (Deep Seismic Sounding) profiles, deep reflection profiles as well as tomographic experiments (Luosto et al. 1984, 1990, 1994; Grad and Luosto 1987; BABEL Working Group 1991; FENNIA Working Group 1998; Heikkinen and Luosto 2000; Hyvönen et al. 2007). Already the first experiments documented five fundamental properties: three crustal layers, high crustal velocities, high velocity lower crust, above-average continental crust thicknesses, and well-reflective crustal and Moho boundaries (Luosto 1984; Luosto et al. 1984). Compilations of the data sets have been presented as maps of the depth to the Moho, thickness of the upper crust and depth to the lower crust, 3D-tomographic models, etc. (Korja et al. 1993; Luosto 1997; Hyvönen et al. 2007). These compilations indicate that although the crust seismically shows a layered structure, horizontal velocity variations point to the crust being assembled of several subblocks, resulting in highly three-dimensional regional crustal structure.

Although the data coverage for large-scale crustal studies is rather good in Fennoscandia, sampling is uneven because most of the experiments have been along NE–SW to N–S directed lines. At the time of the data collection, it was believed that the lines were directed across the general orogenic strike. Only after the large-scale deep seismic reflection experiment FIRE (Finnish Reflection Experiment; Kukkonen and Lahtinen 2006; Korja and Heikkinen 2008), it became evident that the orogenic strike may have

¹ Department of Geosciences and Geography, University of Helsinki, PO. Box 68, 00014 Helsinki, Finland. E-mail: timo.tiira@helsinki.fi

² Institute of Geophysics, Polish Academy of Sciences, Ks. Janusza 64, 01-452 Warsaw, Poland.

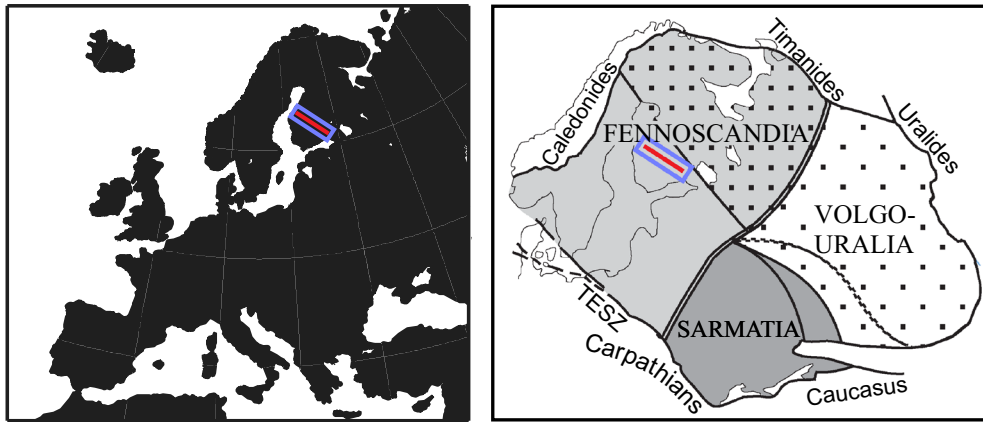


Figure 1

Location of KOKKY line within the simplified geological framework of Europe. Craton map modified after Bogdanova (1993)

varied during the accretionary process and that in central Finland the main strike direction is actually NE–SW. Thus, most of the previous surveys have been conducted along rather than across the strike. This implication is also supported by the regional-scale tomographic model that shows large-scale horizontal variations in NW–SE direction (Hyvönen et al. 2007). To improve the quality of the crustal layer interpolations and tomographic models, DSS lines in NW–SE direction are needed.

General tectonic and geological framework of southern and central Finland was formed in the multiphase Paleoproterozoic (1.92–1.79 Ga) accretionary Svecofennian orogeny (e.g. Lahtinen et al. 2009). The Svecofennian bedrock was amalgamated from several Paleoproterozoic micro-continental blocks, island arcs, and associated basins that were accreted to the margin of the Karelian continent in several phases. The accretionary stage was followed by phases of orogenic collapse, lithospheric extension, and cratonic stabilization, which largely overprinted the previously generated collisional structures. Roughly 100 million years after the cessation of plate tectonic activity, the Svecofennian tectonic province was perturbed by a series of at least seemingly anorogenic magmatic events at ca. 1.65–1.53 Ga, which generated large volumes of rapakivi granites and related rock types such as gabbros and anorthosites, which sharply cross-cut the

regional orogenic fabric in Southern Finland (e.g. Rämö and Haapala 2005; Heinonen et al. 2017).

The 490 km long Kokkola–Kymi seismic reflection line (KOKKY profile) runs in NW–SE direction and transects the Western and Southern Finland arc complexes that form the Western (WFS) and Southern Finland subprovinces (SFS) of the Svecofennian tectonic regime (Nironen 2017). It also transects the major Proterozoic crustal units identified on a tomographic velocity model (Hyvönen et al. 2007) and the most prominent crustal thickness anomalies identified on a Moho depth map (Grad et al. 2009). KOKKY line was designed to run perpendicular to the orogenic strike in WFS and the suture between WFS and SFS, to connect and transect existing DSS lines SVEKA81, BALTIC (Luosto et al. 1990), FIRE1 and FIRE2 and to be partly parallel to FIRE3A (Kukkonen and Lahtinen 2006). The furthest shots that could reliably be located came from near Vyborg, and there were no receivers on the Russian side. The purpose of the line was to study the regional-scale velocity variation in central and southern Finland and its association with paleosutures and terrane boundaries. For this purpose we verified the horizontal velocity anomalies in NW–SE direction indicated by the tomographic interpolations. We studied possible velocity anisotropy to compare the velocity variations with the reflection properties of the FIRE3A. The part where KOKKY and FIRE3A are parallel is 210 km in

length, including parts of Bothnian belt and Central Finland granitoid complex (Fig. 2).

Controlled source seismology (e.g. Malinowski 2013; Spada et al. 2013) is one of the main tools used in Earth imaging, especially when aiming towards the middle and lower crust structures, Moho topography and velocities in the lithospheric mantle. Data for such studies are acquired during campaigns on wide-angle reflection and refraction (WARR) profiles (also called deep seismic soundings, or DSS profiles), which are hundreds of kilometres long and require strong explosive sources such as TNT. Given the cost of such experiments, difficult logistics, and the strict regulation on experiments involving explosives in the ground, a more cost-efficient approach was used in this study. Therefore, sources of signals in this study are blasts from quarries and road construction sites along the predetermined profile. This is convenient because quarries require tons of explosive material each week and their functionality in seismic experiments had been previously successfully tested in association with the HUKKA2007 project (Tiira et al. 2013).

2. Geological and Geophysical Background

The NW–SE oriented KOKKY profile studies the crustal structure of the Paleoproterozoic Svecofennian province and crosses over from the WFS to the Southern Savo nappe system. Possibly it also goes across the suture between WFS and SFS (Nironen 2017) at a high angle. The profile images the Bothnian belt (BB) and Central Finland granitoid complex (CFGC) of the WFS and the Southern Savo nappe and Saimaa area of the SFS (see Nironen 2017 for nomenclature) as well as the Wiborg rapakivi batholith (WRB; Fig. 2).

The Bothnian belt represents an accretionary prism of an arc complex. It is composed of metapelites and metagreywackes and minor mafic metavolcanic units that have been deformed and metamorphosed under high temperature–low pressure conditions. It consists of schists, black schists, gneisses, migmatites, and granitoid plutons (e.g. Mäkitie et al. 1999; Suikkanen et al. 2014; Kotilainen et al. 2016a, b; Hölttä and Heilimo 2017). FIRE3A reflection seismic profile (Sorjonen-Ward 2006)

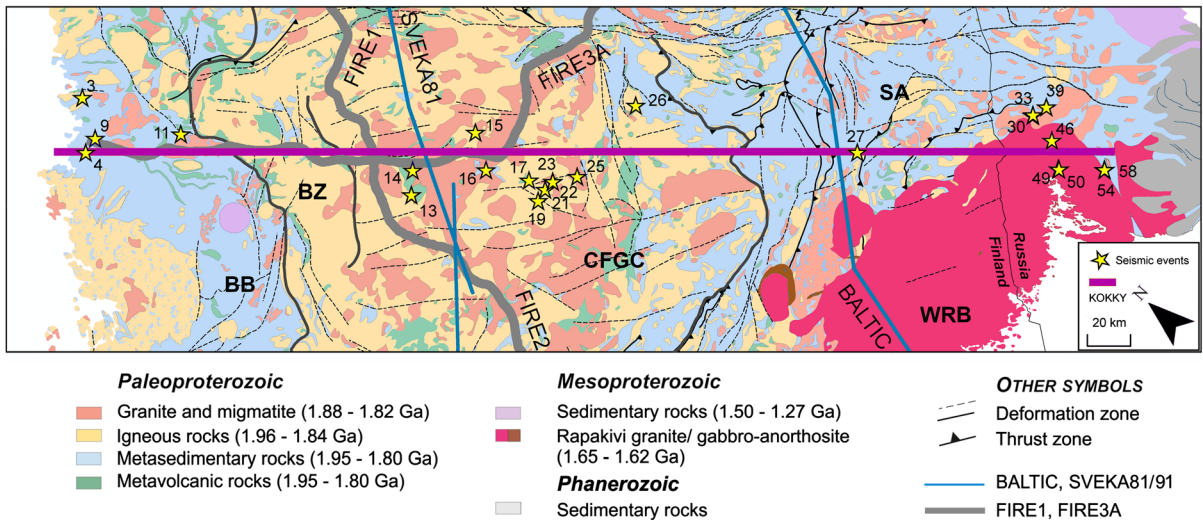


Figure 2

A map of the bedrock geology and main upper crustal tectonic units along KOKKY profile (purple line). Shot points used for ray tracing are shown with numbered stars. Thin blue lines indicate locations of BALTIC and SVEKA81 profiles (Luosto et al. 1990) and thick gray lines show locations of FIRE profiles (Kukkonen and Lahtinen 2006; Korja and Heikkinen 2008). SVEKA91 profile (Luosto et al. 1994), a southern continuation of SVEKA81, crosses SVEKA81 but it does not cross KOKKY. Color codes of geological units in the Russian territory (the eastern end of the profile) are similar to those on the Finnish side but fault lines are shown on the Finnish side only. BB Bothnian belt, BZ boundary zone, CFGC Central Finland granitoid complex, HB Häme belt, SA Saimaa area, WRB Wiborg rapakivi batholith. For numeric values of all shot locations, including those unused for ray tracing, see Table 1

Table 1
Velocity model used at Institute of Seismology, University of Helsinki

V_p	V_s	Depth range
6.19	3.60	0–15 km
6.70	3.84	15–40 km
8.03	4.64	40 km →

parallel to the KOKKY line revealed east–southeast dipping reflectors that have been correlated with the contacts of the supracrustal units on the surface. These reflectors transect the present-day middle crust and are interpreted as marking the contacts of the Bothnian belt blocks with each other and the associated Pirttikylä block towards CFGC. Tectonic interpretations based on field observations suggest the reflectors to be thrusts or stacking surfaces (Sorjonen-Ward, 2006) and analogue modelling suggests them to be thick-skin stacking structures that reactivated as large normal faults during extensional collapse (Nikkilä et al. 2015).

CFGC is a large upper crustal granitoid batholith (Elliott 2003; Nironen 2017) intruded into a deformed and metamorphosed arc complex. It consists mainly of granitoid plutons together with minor amounts of gabbroic plutons and mafic dykes, and less prominently of volcano-sedimentary units (Nironen 2017). Nikkilä et al. (2016) suggested that the batholith was formed in three stages involving mafic underplating, differentiation, partial melting, and granitoid formation. By using FIRE1 and FIRE3A transect data and analogue modelling techniques, Nikkilä et al. (2015) interpreted that the orogenic crust has laterally extended by 50% and thinned by maximum of 20% via westward gravitational spreading. The current erosional level of the orogen is 15–20 km and metamorphic degree is high (Hölttä and Heilimo 2017). Based on the more juvenile isotopic character of the granitic rocks and the presence of larger amount of mafic rocks, Lahtinen et al. (2016) also defined a separate boundary zone (BZ) on the northwestern flank of CFGC between BB and the bulk of CFGC (Fig. 2).

Southern Savo nappe system is a late allochthonous unit partly thrust on WFS (Nironen 2017) and thus covers the suture between WFS and SFS. The Saimaa

area of SFS is composed of metasedimentary rocks with highly varying passive margin to island arc geochemical character (Lahtinen et al. 2010). Towards the south, the metasediments have been strongly migmatized at 1.84–1.81 Ga (Kähkönen 2005) and they form large intrusions of migmatitic granites belonging to the Southern Finland granite suite.

The Wiborg suite granites belong to the largest rapakivi intrusion of southern Finland, the Wiborg batholith that intruded SFP and the Saimaa area at around 1.63 Ga (Rämö and Haapala 2005; Heinonen et al. 2016, 2017). The majority of the batholith comprises massive and rather monotonous alkali feldspar megacrystic (wiborgitic) rapakivi granites but the northeastern part on the Finnish side of the border is more heterogeneous and consists of both diverse types of rapakivi granites and heterogeneous blocks of the country rocks included in the rapakivi granite as megaxenoliths (Vorma 1975; Rämö and Haapala 2005; Harju et al. 2010). Previous seismic interpretations on the upper crustal structures beneath the Wiborg batholith suggest that the granites are underlain by a layer of more mafic material at the depths of ca. 15–25 km, potentially consisting of anorthositic rocks (Elo and Korja 1993; Rämö and Haapala 2005).

3. Data Acquisition

KOKKY line was designed as a test environment for low-cost lithospheric studies and relies purely on industrial blasts. It crosses pre-existing SVEKA81 (Luosto et al. 1984), BALTIC (Luosto et al. 1990) and FIRE1 profiles and is partially parallel to deep reflection profile FIRE3A (Kukkonen and Lahtinen 2006). The profile starts on the coast of Bothnian Bay and runs NW–SE for nearly 500 km southeast towards eastern end of the Gulf of Finland (see Figs. 1, 2 for location). Its acquisition program was split into two summer campaigns. In year 2012, the Kokkola–Äänekoski (NW) transect was surveyed, followed by Karstula–Nuijamaa (SE) transect in 2013. The overlap between deployments was 60 km. In the first campaign, 49 portable seismic stations were deployed, and in the second campaign, 74 stations were deployed. The type of all temporary seismic equipment was Trimble Ref Tek 125

Full-Scale Crustal Interpretation of Kokkola–Kymi (KOKKY) Seismic Profile

Table 2

Details of shots used to construct KOKKY profile

Shot number	Latitude (°)	Longitude (°)	Distance from beginning of line (km)	Offset from line (km)	Date	Time in UTC
1	22.7153	63.7134	6.61	22.77	12.7.2012	14:31:14.27
2	22.716	63.7102	6.88	23	27.6.2012	17:03:17.64
3*	23.5097	63.973	13.21	25.43	13.8.2012	15:34:15.24
4*	23.1585	63.8036	14.76	0.11	10.5.2013	09:48:13.31
5	22.9246	63.6538	18.61	20.06	13.8.2012	12:32:43.42
6	22.9248	63.6538	18.62	20.05	20.7.2012	10:33:50.03
7	23.3152	63.8172	19.05	6.48	4.6.2013	11:08:31.73
8	23.3153	63.817	19.07	6.47	28.5.2013	15:06:26.96
9*	23.3158	63.8168	19.11	6.47	13.6.2013	08:01:24.23
10	23.0735	63.6922	20.71	11.79	27.6.2012	14:46:13.65
11*	23.9012	63.5737	58.72	8.57	3.7.2012	14:33:37.00
12	23.8791	63.2102	87.3	20.19	10.7.2012	09:41:58.70
13*	24.9436	62.7025	165.54	19.46	28.6.2012	08:44:47.35
14*	25.1148	62.7685	166.05	8.04	15.5.2013	09:57:53.73
15*	25.7511	62.6818	195.08	9.57	2.8.2012	09:59:59.88
16*	25.5628	62.5443	199.99	7.88	31.7.2012	11:32:36.63
17*	25.7552	62.3832	219.97	12.52	24.5.2013	08:15:58.06
18	25.6736	62.2995	224.08	21.9	23.5.2013	10:12:39.42
19*	25.6736	62.2982	224.19	22	8.5.2013	09:32:10.82
20	25.7893	62.3089	227.31	16.74	9.7.2012	10:42:16.30
21*	25.7891	62.3076	227.42	16.85	27.6.2012	10:24:47.09
22*	25.8878	62.307	230.88	13.08	7.6.2013	06:22:20.48
23*	25.8864	62.3062	230.9	13.19	20.7.2012	08:48:21.58
24	25.9735	62.2178	241.26	16.38	8.5.2013	08:32:21.40
25*	26.0648	62.2447	242.18	10.84	15.5.2013	07:26:28.83
26*	26.8873	62.2584	269.25	22.27	13.6.2013	10:25:56.26
27*	27.8414	61.4325	371.87	0.66	21.5.2013	09:02:51.90
28	28.1829	61.0339	417.7	13.81	15.5.2013	10:33:11.67
29	28.1833	61.0289	418.15	14.15	29.5.2013	10:33:17.10
30*	29.0484	60.9699	452.97	17.84	7.8.2012	08:06:32.30
31	29.0484	60.9699	452.97	17.84	8.8.2012	10:23:43.84
32	29.0504	60.9691	453.11	17.87	1.8.2012	08:25:26.10
33*	29.0554	60.9707	453.14	18.19	15.5.2013	09:32:57.90
34	29.1634	60.9522	458.42	21.44	17.5.2013	10:32:56.40
35	29.1654	60.9514	458.56	21.47	24.5.2013	07:59:38.61
36	29.1687	60.9498	458.81	21.49	31.5.2013	08:35:06.95
37	29.1694	60.9487	458.93	21.45	29.5.2013	11:53:33.63
38	29.1743	60.9484	459.12	21.63	28.6.2012	10:02:40.50
39*	29.1795	60.9483	459.31	21.84	5.6.2013	09:37:50.71
40	29.1795	60.9475	459.38	21.79	17.5.2013	10:07:55.60
41	29.1832	60.947	459.55	21.91	30.5.2013	07:59:28.68
42	29.1859	60.9478	459.57	22.08	16.5.2013	11:49:13.42
43	29.182	60.9462	459.58	21.8	28.5.2013	13:15:02.53
44	29.183	60.9444	459.77	21.72	8.5.2013	09:33:20.71
45	28.9724	60.8443	461.23	5.81	29.5.2013	08:05:34.66
46*	28.988	60.843	461.88	6.37	15.5.2013	09:21:13.42
47	29.2724	60.9303	464.04	24.51	22.5.2013	11:01:38.00
48	29.2746	60.9304	464.1	24.61	14.6.2013	09:07:47.09
49*	28.8335	60.7475	464.81	6.88	24.5.2013	10:28:54.83
50*	28.8362	60.745	465.12	6.94	8.5.2013	10:26:19.36
51*	28.8355	60.7445	465.14	7	14.6.2013	10:11:16.01
52	28.8391	60.7432	465.38	6.94	29.5.2013	09:49:42.24
53	29.0743	60.5998	485.89	7.06	4.7.2012	11:14:08.80
54*	29.0731	60.597	486.09	7.31	15.5.2013	09:50:34.17

Table 2 *continued*

Shot number	Latitude (°)	Longitude (°)	Distance from beginning of line (km)	Offset from line (km)	Date	Time in UTC
55	29.078	60.597	486.26	7.1	22.5.2013	08:08:36.06
56	29.0836	60.5992	486.27	6.7	29.5.2013	15:10:51.97
57	29.0784	60.597	486.28	7.08	17.5.2013	16:08:05.23
58*	29.078	60.5968	486.28	7.11	11.6.2013	11:41:00.14
59	29.0781	60.5967	486.29	7.11	14.6.2013	08:15:19.96
60	29.0925	60.5956	486.89	6.58	22.5.2013	09:03:11.52
61	29.0704	60.5769	487.74	8.83	7.6.2013	08:07:33.63
62	29.0696	60.5765	487.75	8.89	10.8.2012	08:11:58.40
63	29.0695	60.5762	487.77	8.92	6.7.2012	08:15:02.80

Not all shots have been used for calculation of models, but only the most reliable ones denoted by asterisks (*) after the shot number

For locations of these shots, see Fig. 1. For locations of shots on a map, see Fig. 1

(Texan). Data from permanent stations (MEF, NUR, PVF and VJF) and one Kouvola temporary network station (KV1) were used as well.

In total, 63 shots from quarry blasts and other explosions were recorded. The initially unknown locations of shots were resolved from the data of the temporary deployment and data of the Finnish National Seismic Network (FNSN; <https://doi.org/10.14470/ur044600y>). With minimum off-the-line shot distance as small as 110 m and maximum of 25.4 km, average perpendicular offset was 14 km. The events were preliminarily located using an ordinary least-squares method included in the HYP locator of SeisAn software (Havskov and Ottemoller 1999). Known locations of quarries and mines, aerial orthomosaics of the National Land Survey of Finland, as well as other digital maps and satellite images were used for verification of shot locations. Events close to any open quarry, mine or construction site were associated with the known location. In most cases the location accuracy was better than 1 km and therefore several shots could be reliably associated with the same site. Finnish shot locations from same sites include shots 1–2 (Alholmen, Pietarsaari), 5–6 (Stormossen, Vaasa), 7–9 (Runtujärvi, Kokkola), 20–21 (Kaakkovuori, Jyväskylä), and 28–29 (Ihalainen, Lappeenranta). On the Russian side the accuracy was typically lower simply due to station geometry—all stations were on the Finnish territory. Therefore, we selected a relatively large number of Russian shots for initial analysis, with the expectation that only the few most reliable ones can be retained.

The most prominent Russian shot locations were western Kamennogorsk (shots 32–33), eastern Kamennogorsk (34–44), Vozrozhdenie (45–46), north of Vyborg (49–52), and Gavrilovo (53–63).

The origin times were estimated by extrapolating station arrivals backwards in time using the predicted traveltimes to temporary and permanent stations and the velocity model used in the daily analysis of seismic events at the Institute of Seismology, University of Helsinki (Table 1). This three-layer model consists of mainly granitic layer (0–15 km), mainly basaltic layer (15–40 km) and mantle. For each source, the mean origin time was estimated by subtracting the travel times derived from ISUH standard travel time tables from the arrivals of each seismic phase and calculating the average and standard error of the mean (σ/\sqrt{N}) for the resulting origin time estimates. However, several explosions at a quarry may take place within a time-frame of seconds, and we only took the picks related to the first explosion into account. Geotool software of CTBTO (<https://www.ctbto.org>) was used for manual phase picking. The origin time was accepted if its standard error of the mean was less than 50 ms and if at least 5–6 phases had been used for location. This left us with 25 events as seen in Fig. 2. Location and event times of all shots are listed in Table 2.

4. Seismic Data

The seismic record sections show good quality both for P- and S-waves. Examples of record sections for

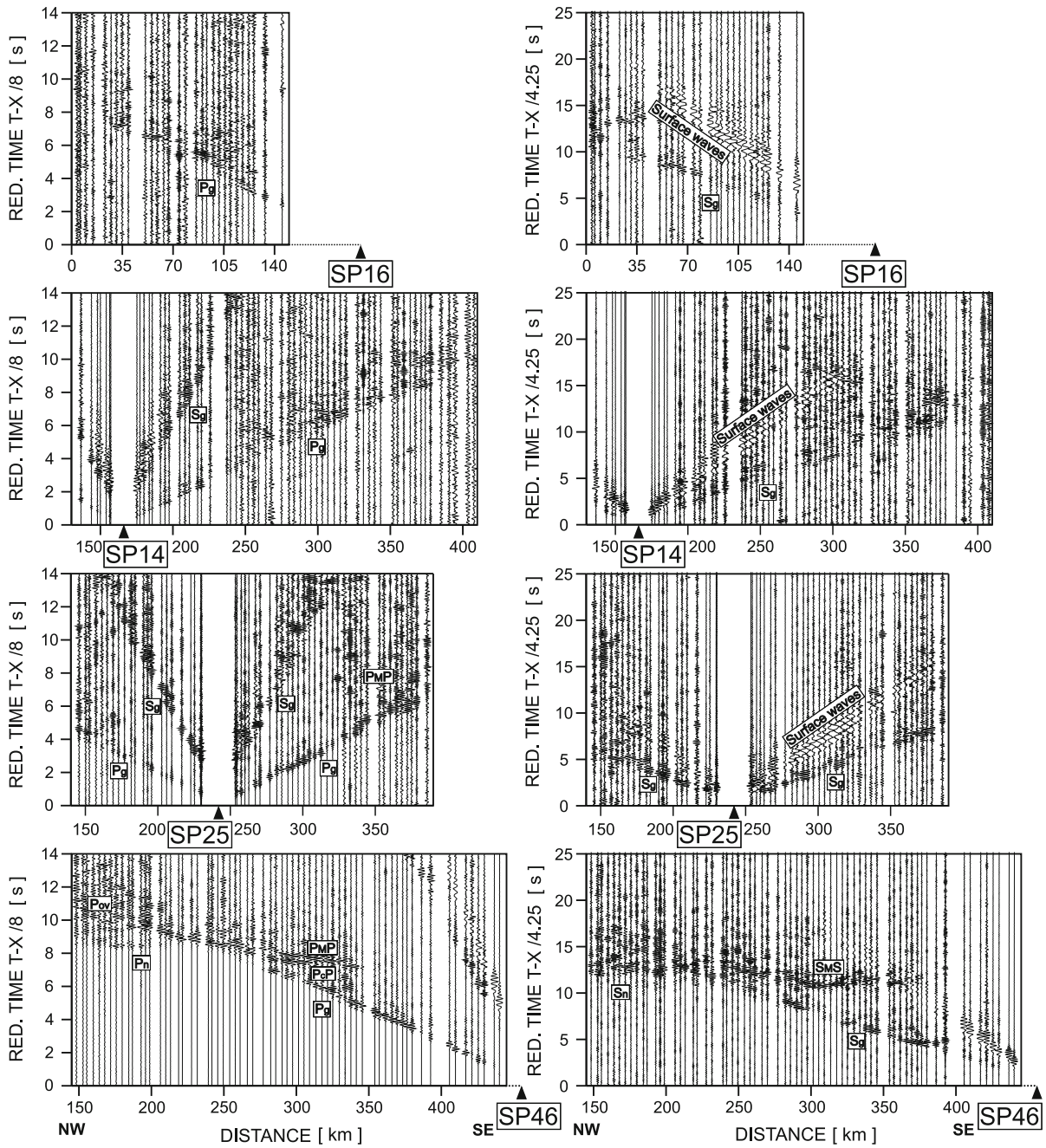


Figure 3

Recorded seismic sections for P-wave (left, with reduced velocity 8 km/s, filtered 2–12 Hz) and S-wave (right, with reduced velocity 4.25 km/s, filtered 1–6 Hz). Bothnian belt, Central Finland granitoid complex and Saimaa area are illustrated in separate subplots and locations of shots 16, 14, 25, and 46 are also shown

P-wave and S-wave are shown in Fig. 3. Only basic bandpass filtering (Butterworth filter) was applied to the

data before picking, 2–10 Hz for P-wave seismic sections and 1–6 Hz for S-wave.

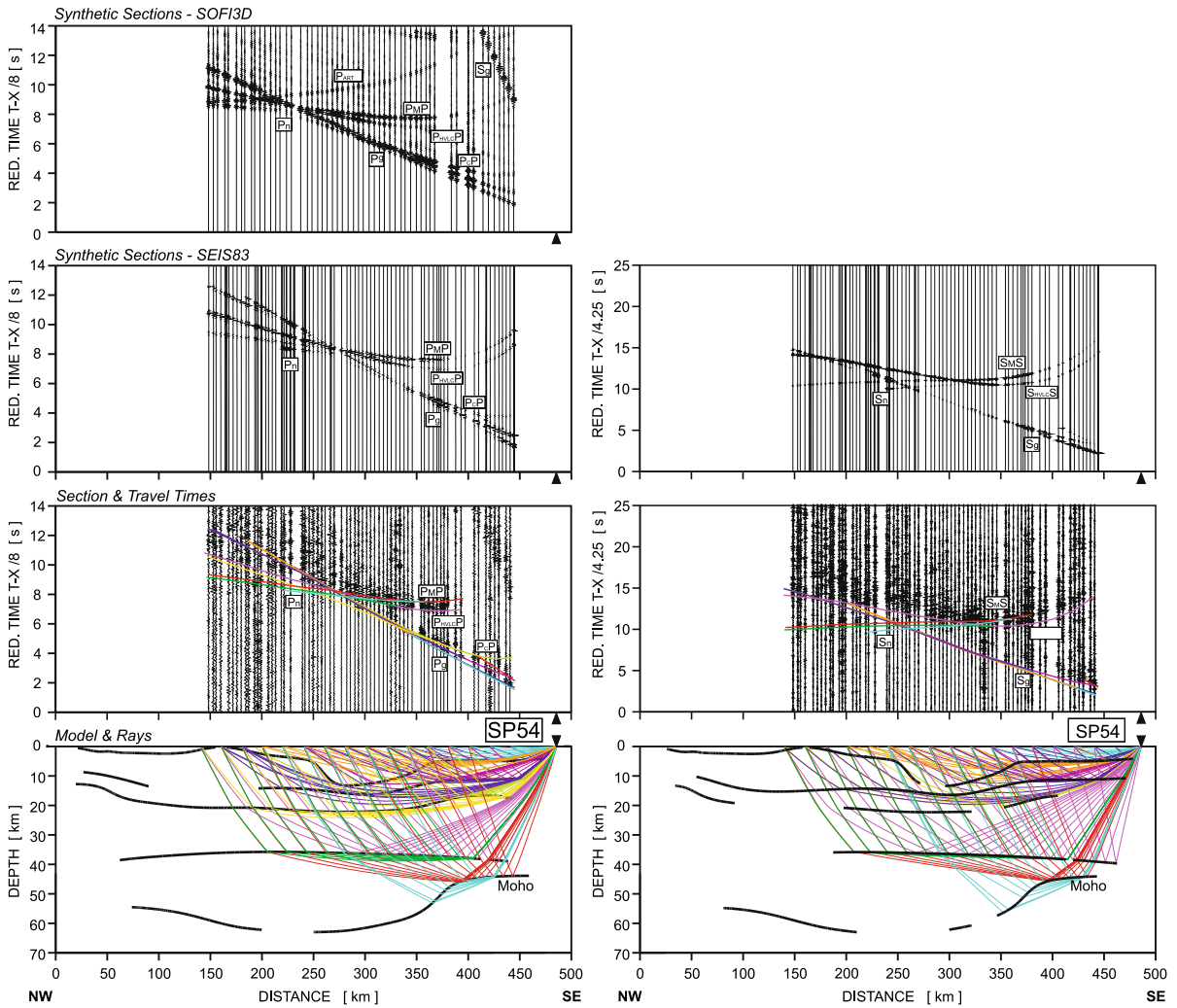


Figure 4
Examples of traveltimes modelling, for P- (left) and S-wave (right) arrivals

4.1. P-Wave Arrivals

Seismic phases corresponding to the first direct arrivals (P_g) with apparent velocities ranging from 5.9 km/s in northwestern part, to 6.0–6.1 km/s in central part, and up to 6.2 km/s in the southeast end are consistent with the expected lithologies in the upper crust (granites and schists) and can be picked at over 210 km long offsets. At far offsets, there is evidence for a high velocity lower crust with apparent

velocity > 7 km/s—see Fig. 3. Mantle propagating waves, refraction under Moho (P_n), are present with apparent velocity 8.2–8.3 km/s.

The Moho reflections ($P_M P$) are strong and easy to interpret. Several mid-crustal reflections ($P_C P$) are distinguishable. Complex reflection pattern is visible in southeastern part of the profile at about 8 s in reduced time (8 km/s) where Moho and upper boundary of the lower crust are only a few kilometers apart (Fig. 4).

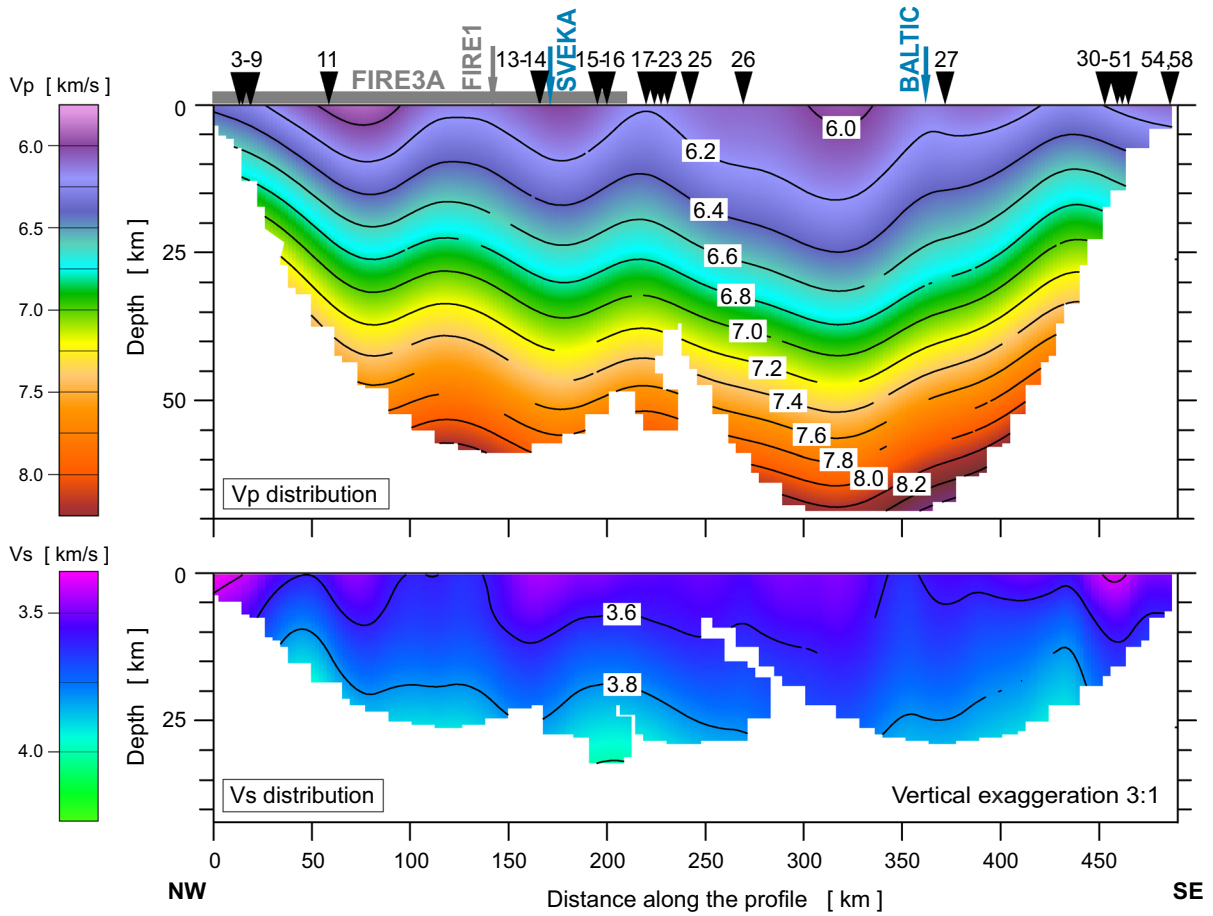


Figure 5

Tomographic 2D models from 3D corridor along the KOKKY profile. Crossing points of FIRE1, SVEKA, and BALTIC profiles are also shown. In its western part, KOKKY is parallel and close to FIRE3A at a distance of 210 km as shown by a solid gray line

4.2. S-Wave Arrivals

The quality of the S-wave record sections is only slightly inferior compared to P-wave sections. The strongest shots generated S_g signals visible for over 300 km. Again, lowest apparent upper crust velocities, 3.4–3.45 km/s, correspond to BB area. Central part of the profile is characterized by upper crust velocities of ~ 3.5 km/s, whereas in SE near-surface velocities reach up to 3.6 km/s. Location of mid-crustal S-wave reflections complies with their distribution for P-wave. Moho shape is relatively well retrieved using $S_{M,S}$ and some details about S-wave velocity distribution in the upper mantle can be resolved using S_n which has apparent velocity of 4.8–4.85 km/s.

5. Seismic Modelling

5.1. Tomography Modelling

Separate P- and S-wave tomographic velocity models were computed using JIVE3D program (Hobro et al. 2003). The program is based on the 2D inversion algorithm by McCaughey and Singh (1997). A non-linear problem is approximated in a sequence of linear steps. An iterative inversion path is used with regularized least-square solution and conjugate gradient method for optimization (e.g. Press et al. 1992) between steps. A linearized, regularized velocity model grid is inverted by optimizing travel times calculated with the model to fit the measured travel time data. Tomographic

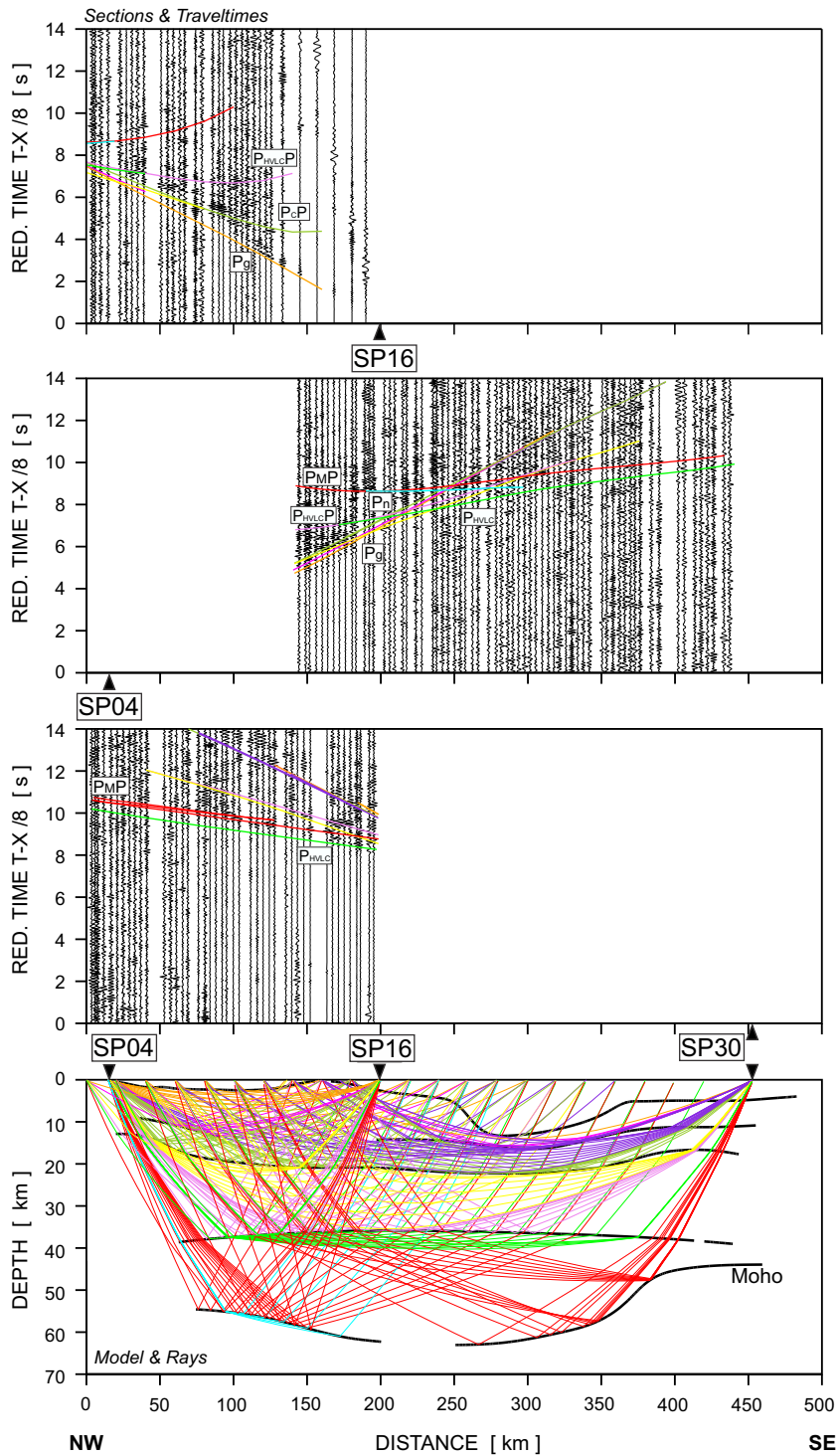


Figure 6

Triple plot of final model to real data fit with P wave ray paths on a model. SP04, SP16 and SP30 refer to shot points 4, 16, and 30

Full-Scale Crustal Interpretation of Kokkola–Kymi (KOKKY) Seismic Profile

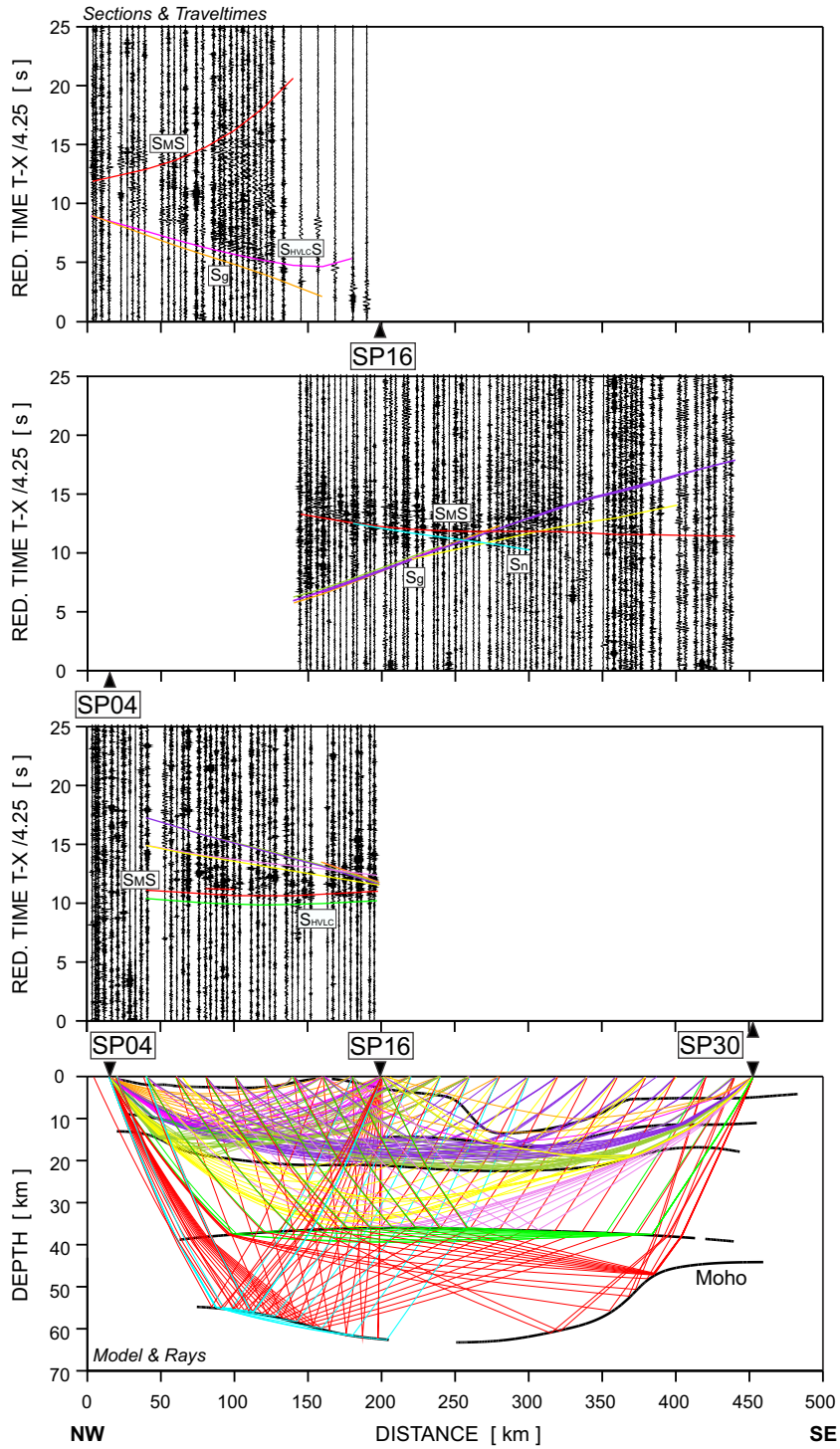


Figure 7

Triple plot of final model to real data fit with S wave ray paths on a model. SP04, SP16 and SP30 refer to shot points 4, 16, and 30

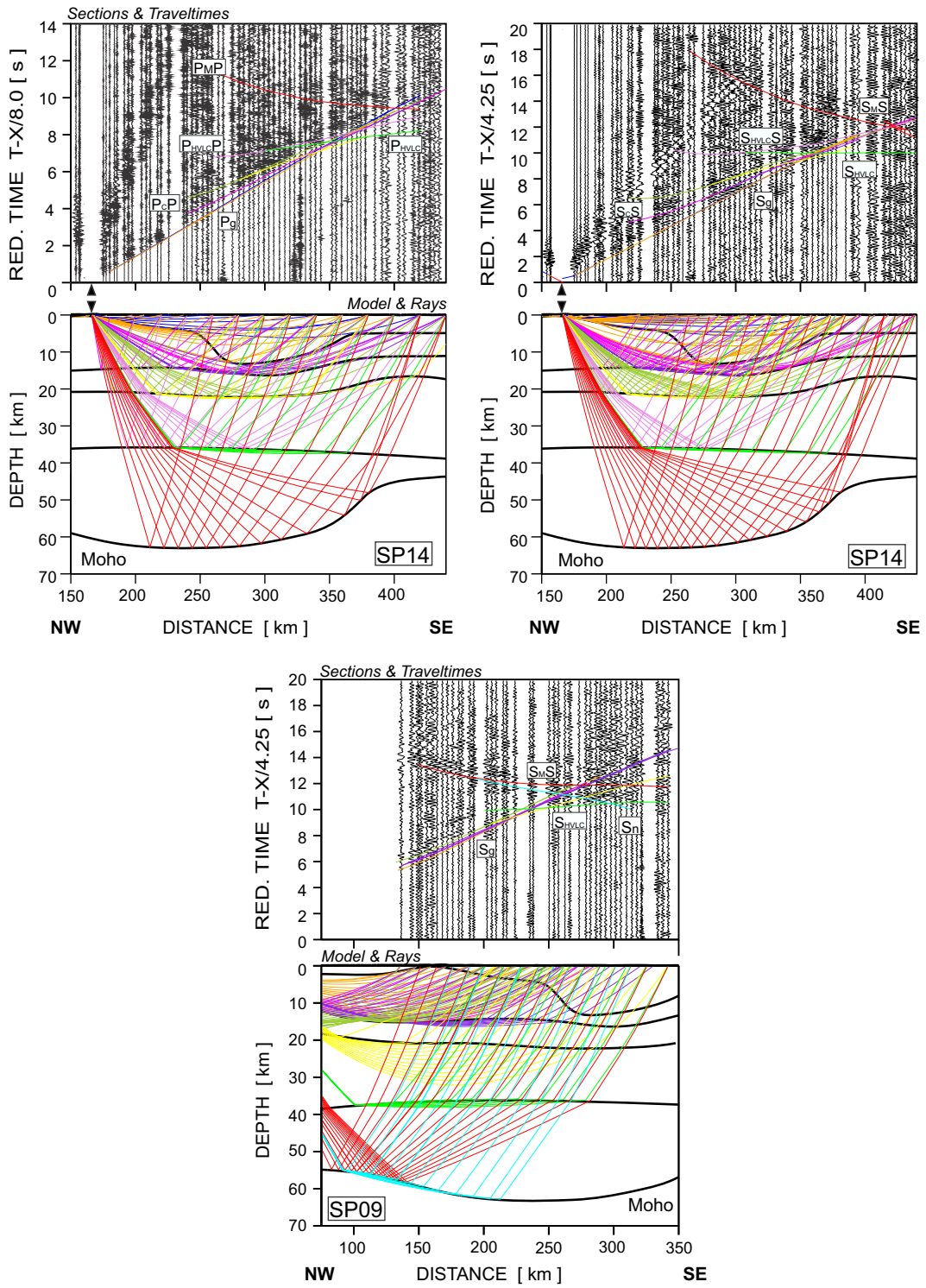
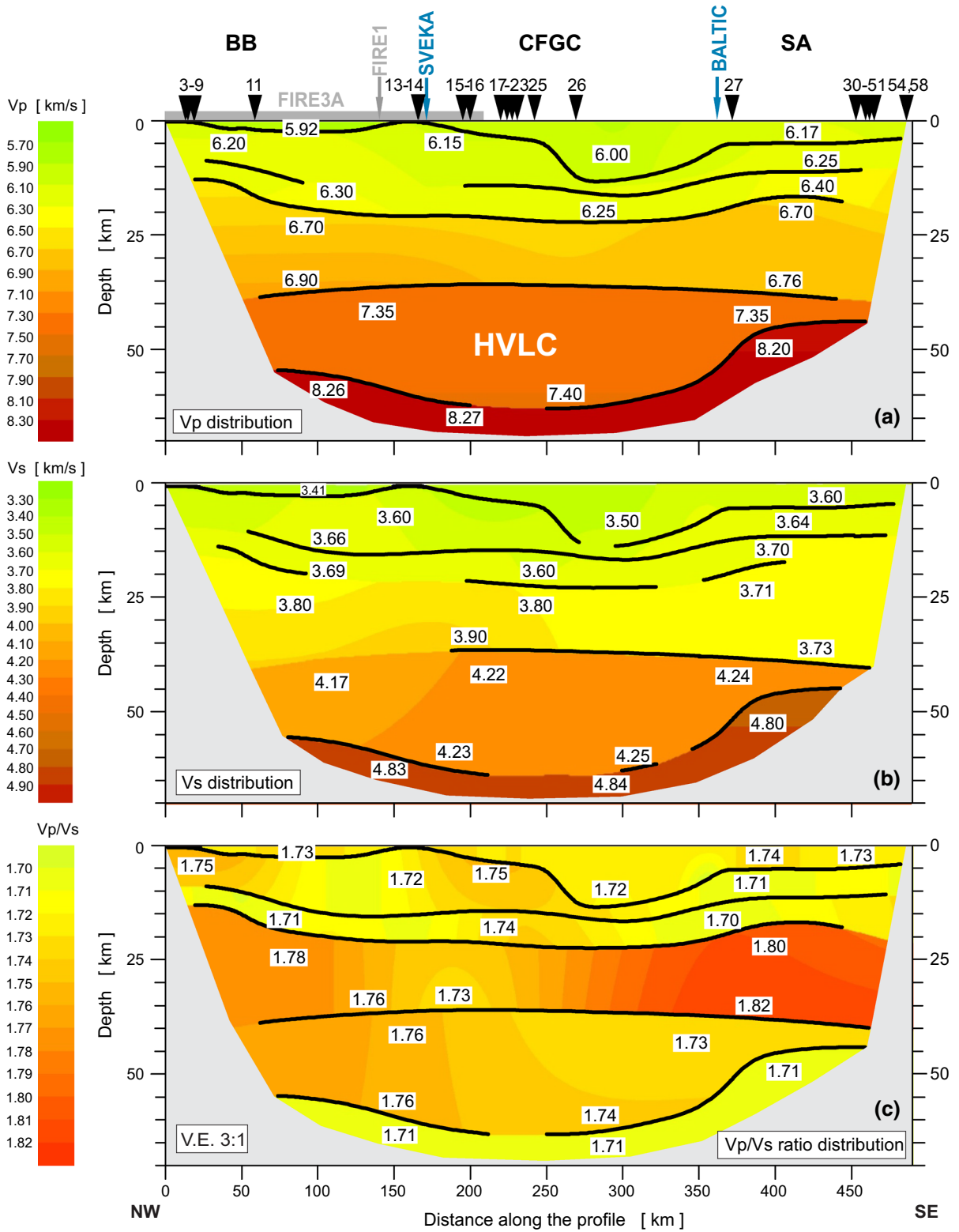


Figure 8

Triple plot of final model to real data fit with P and S wave ray paths on a model. SP14 (P_MP and S_MS) and SP09 (S_n) refer to shot points 14 and 9

Full-Scale Crustal Interpretation of Kokkola–Kymi (KOKKY) Seismic Profile



◀Figure 9

Final two-dimensional seismic models of P-wave velocity V_p , S-wave velocity V_s , and distribution of V_p/V_s ratio. Confirmed boundaries are displayed with solid black lines. Numbered triangles indicate shot numbers. Crossing points of FIRE1, SVEKA and BALTIC profiles are also shown. In its western part, KOKKY is parallel and close to FIRE3A at a distance of 210 km as shown by a solid gray line. *BB* Bothnian belt, *CFGC* Central Finland granitoid complex, *HVLC* high velocity lower crust, *SA* Saimaa area, *V.E.* vertical exaggeration

inversion (Hobro et al. 2003) results in smooth velocity models by automatically adjusting seismic velocities in a regular grid. Inverted models typically have minimal structures since adjustments are gradual and the algorithms cannot by default accommodate big shifts in velocities.

Only refracted crustal turning waves were used in this study. The models were solved in 50 km wide, 492 km long and 80 km deep 3D corridor and the number of used shot records was 25. Some shots were disregarded since there were multiple shots at the same quarry. Number of P-wave picks was 1875 and that of S-wave picks 963. The maximum source–receiver distance for rays to reach the target receivers was less than 300 km, meaning that the use of flat earth assumption and the Cartesian coordinate system was sufficient (Ollikainen and Ollikainen 2004). Figure 5 shows 2D models from 3D corridor along the main KOKKY profile line. The velocity fields of the tomographic models were used as starting points in the ray tracing modelling. The method alone was not sensitive enough to provide information on inhomogeneities across (perpendicular to) the 3D corridor.

5.2. Ray tracing modelling

The SEIS83 package (Červený and Pšenčík 1984) and graphical interfaces MODEL (Komminaho 1998) and ZPLOT (Zelt 1994) were used for forward traveltimes modeling. The SEIS83 package was used to calculate ray paths, traveltimes, and synthetic seismograms seen in Figs. 3, 4, 6, 7, and 8. The final models were compiled using trial-and-error forward modeling guided by a priori knowledge of source locations. In iterative process, traveltimes calculated

for current velocity model were compared with observed, and corrected towards misfit minimization. Due to preferential horizontal propagation of rays, velocities were typically averaged laterally. Synthetic seismograms were calculated for qualitative control over modeled and observed amplitudes. Additionally, the input model was supplemented by the data from partially parallel FIRE3 profile and information from crossing profiles SVEKA81, BALTIC and FENNIA (Janik et al. 2007; Janik 2010; Kukkonen and Lahtinen 2006). The two-dimensional forward modeling with ray tracing method resulted in P-wave velocity distribution model shown in Fig. 9a. Figure 4 provides general overview of modeling including ray-paths, synthetics and overall fit to experimental data. Figure 6 provides another insight into modeling results for three different seismic record sections (shots 4, 16, and 30), supplemented by joint rays diagram on the final model.

Starting with general geophysical assumptions, P-wave velocity model was converted into the S-wave model based on average V_p/V_s ratios ($\sqrt{3}$) for corresponding individual layers in the crossing profiles. Then, the velocity modeling was performed iteratively, constraining the boundaries from P-wave model, until the least misfit of S-wave. Figure 7 gives the overview of the S-wave modeling, the way Fig. 6 does for P-wave. Final S-wave velocity model is shown in Fig. 9b.

By dividing the modelled V_p by V_s models it was possible to obtain the distribution of crustal V_p/V_s ratio along KOKKY line (Fig. 9c). The P-wave and S-wave models in Fig. 9 display only those parts of crustal discontinuities, which were the source of clearly reflected rays. The V_p/V_s ratio model has both P-wave and S-wave model boundaries marked.

5.2.1 P-Wave Velocity Model

The uppermost crust is characterized by velocities ranging from 6.05 to 6.20 km/s. BB, hosting schists and gneisses, has slightly slower velocities of 5.92 km/s than CFGC, hosting mostly granitoid plutons, where higher surface velocities of 6.0–6.1 km/s are observed. Further southeast, both the Häme migmatite belt and Wiborg rapakivi batholith appear to be undistinguishable based on

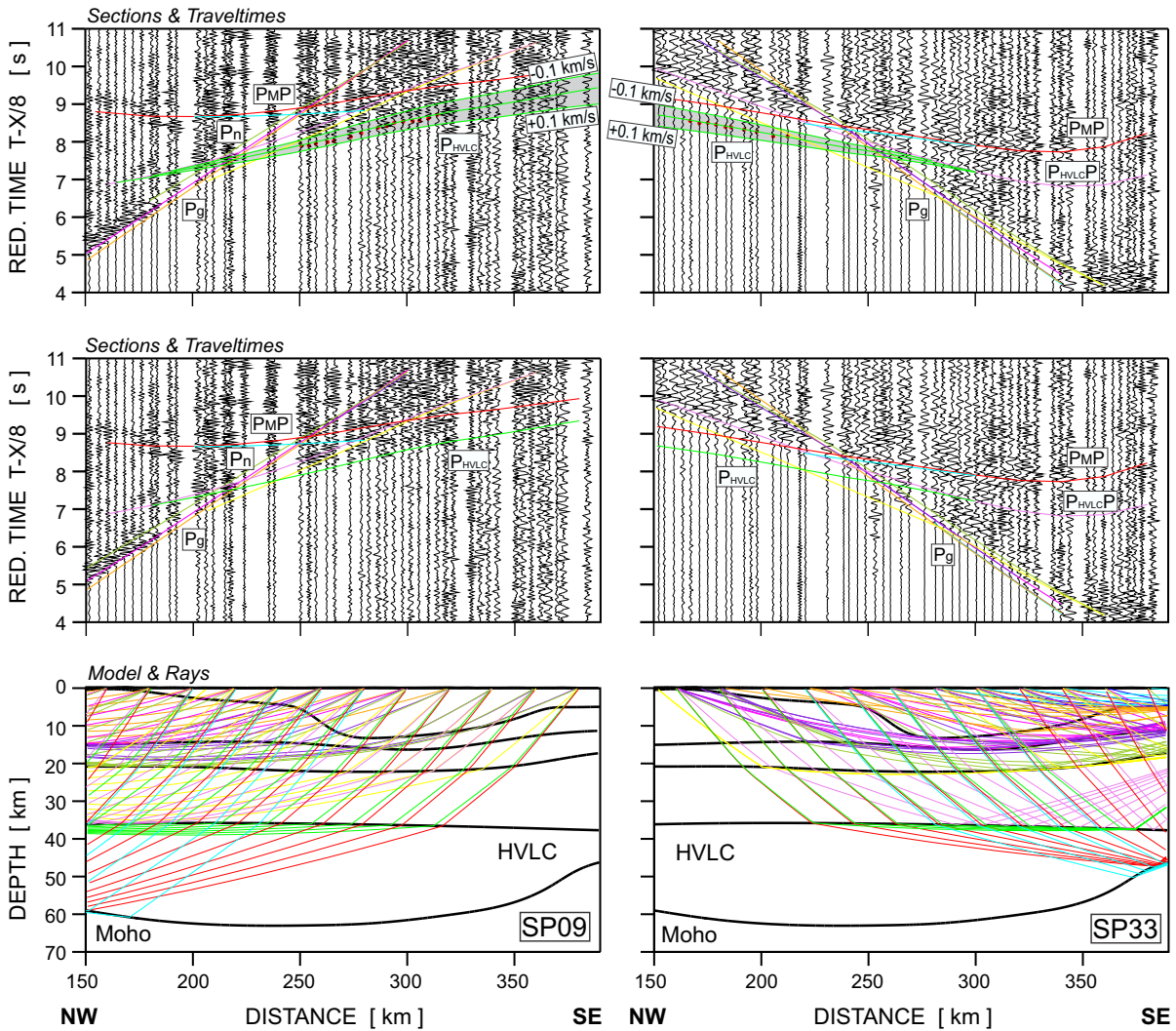


Figure 10

Double plot of final model to real data fit with P_{HVLC} wave ray paths on a model. SP09 and SP33 refer to shot points 9 and 33. Top diagrams present test of the accuracy calculated for P_{HVLC} arrivals for respectively record section. The arrival time of the P_{HVLC} wave was calculated with the estimated velocity of 7.35 km/s and for changes of ± 0.1 km/s. Red dots with size 0.1 s show our picked travel times

V_p values, which grow gradually from 6.15 up to 6.2 km/s. Deeper upper crust may be divided into three parts: NW, central, and SE. Central part has the slowest P-wave velocities of 6.15–6.25 km/s, whereas NW part shows velocities from 6.2 to 6.3 km/s. SE part has the fastest lower upper crust with V_p from 6.2 to 6.4 km/s.

Middle crust is thickening and shallowing towards BB, where it starts at 13 km depth. It gradually deepens towards the center of the profile and reaches

about 21 km depth. After 350 km of the profile the middle crust begins to thicken again up to 16 km at the SE end of the profile. After 450 km it is unknown whether middle crust deepens significantly or only undulates locally due to lack of stations. Although the shape of the middle crust is symmetrical, the velocity distribution is slightly different in eastern lower parts, being over 0.15 km/s faster than average 6.7–6.8 km/s in most of the line.

The high velocity lower crust with homogeneous velocity, ranging 7.35–7.4 km/s, is well documented on a few earlier seismic sections. Figure 10 shows the results of P_{HVLC} modelling for in opposite directions travel times of SP09 and SP33. The top diagram of the Fig. 10 presents results of the accuracy test of our model for P_{HVLC} for both record sections. The arrival time of the P_{HVLC} wave was calculated with the estimated velocity of 7.35 km/s, as well as with velocity modified by ± 0.1 km/s. Red dots show the picks. It is clear from the figure that the uncertainties of velocity determinations are lower than ± 0.1 km/s. Top of HVLC is at an average depth of ~ 38 km, with the shallowest point at ~ 36 km in the central part of the profile and the deepest at ~ 39 km, at both ends of the modelled boundary. The thickness of the high velocity lower crust varies significantly. Layer is thickening from 4 km in SE part of the profile, below the Wiborg batholith, reaching 18 km in its central part corresponding to lower crust of CFGC, and then thinning again to about 12 km in NW part, below BB.

Moho depth varies significantly, from 54 km near the Gulf of Bothnia to 63 km in the middle of the profile, and up to 43 km in Saimaa area. Between areas of deepest Moho, a 55-km section exists where Moho is poorly resolved. However, the maximum depth exceeds the depth range of Grad et al. (2009). Upper mantle in easternmost part is characterized by velocities of ~ 8.17 km/s, which are growing towards the west. In the area of the deepest boundary, velocities underneath the Moho are as high as ~ 8.27 km/s. Below BB the uppermost mantle velocities are about ~ 8.22 km/s.

5.2.2 S-Wave Velocity Model and V_p/V_s Ratio

Upper crustal S-wave velocity variations follow distribution pattern of the P-wave velocities near the surface, showing velocities of 3.4 km/s for NW part of the profile, 3.5 km/s for central part and 3.6 km/s for SE part. Upper crust has velocities between 3.55 km/s and 3.65 in NW part, from 3.5 km/s to 3.6 km/s in central part and around 3.65 km/s in SE part of the profile. Vertical velocity variation is less distinct in subsequent layers. The

deepest upper crust, set in the central part of the profile, is also the slowest one.

In the S-wave velocity field, the sharp contrast between velocities of upper and middle crust occurs only in the central part of KOKKY profile. There, the layers are separated with the V_s contrast of 0.2 km/s, while for the rest of the line the transition is smooth. The less distinguishable middle crust is characterized by velocities from 3.70 to 3.85 km/s in the NW end, just above the 3.7 km/s in the SE end and reaching 3.8 km/s to 3.9 km/s in the central part. Middle crust underneath the Saimaa area is the zone of the greatest V_p/V_s ratio, where its value exceeds 1.80, while it generally remains closer to the range of 1.73–1.76 (see Fig. 9c). Lower crust appears as less uniform with velocities 4.22–4.25 km/s in central and SE part of the line, while NW part is distinctly slower with average velocity 4.17 km/s.

The high velocity lower crust is much less uniform in the S-wave velocity distribution if compared to P-wave model. Its top has the lowest S-wave velocity of 4.17 (may be > 4.15) km/s in the NW part, around 4.2 km/s in the central part and increases up to 4.25 km/s towards the SE end of the profile. This pattern is followed with V_p/V_s ratio, which is the highest in BB area with 1.77, varied in the middle with average ratio of 1.74 and 1.73 in the east. At the bottom of the high velocity lower crust the S-wave velocity increases from 4.2 km/s in the NW part to 4.25 km/s in the SE part.

The shallowest/uppermost upper mantle, present locally at 43 km, is characterized by velocities > 4.75 km/s. Its velocities are growing uniformly at rate ~ 0.05 km/s per 20 km, giving average velocity of > 4.8 km/s in the deepest central part of KOKKY profile and 4.81 in BB, where it reaches depths of 54 km. Upper mantle is characterized by the constant V_p/V_s ratio what gives V_s in between 4.80 and 4.85 km/s, depending on the depth. The high V_p/V_s at SE corresponds to the Wiborg rapakivi area, where Luosto et al. (1990), Hyvönen et al. (2007) and Janik (2010) also found large values in his analysis of BALTIC profile. Also, our observation of lower velocity ratio in the Bothnian schist belt is in agreement with that of Hyvönen et al. (2007) who built a 3D tomographic model for 700×800 km² of central Fennoscandian shield,

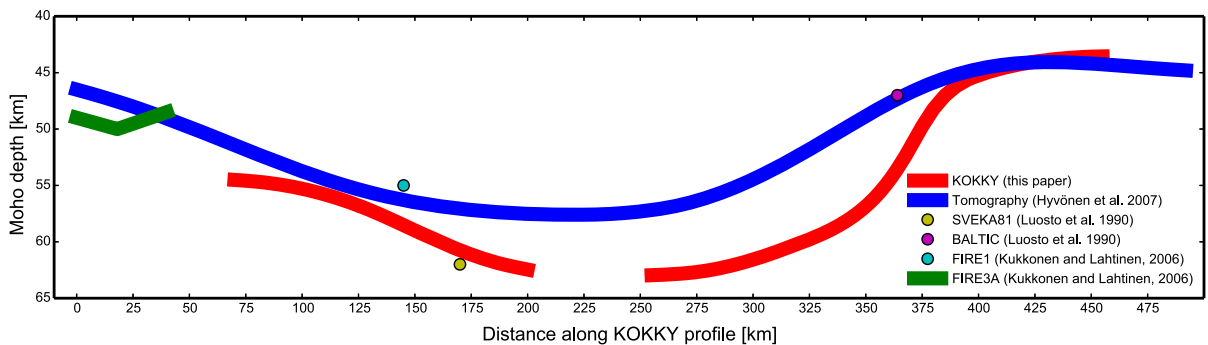


Figure 11

Comparison of the Moho depths from DSS profiles parallel to or crossing KOKKY and Moho depth from tomographic model of Hyvönen et al. (2007). In the FIRE3A section parallel to KOKKY, Moho reflection is evident only in the westernmost 40 km part

using data from SVEKA81, BALTIC, SVEKA91, and FENNIA DSS profiles. The DSS data with dense station spacing had stronger influence than SVEKA-LAPKO data set on the results near the DSS profiles. This explains the similarity between the tomography model and DSS profile Moho depths in Fig. 11. Thus, Fig. 11 of Moho depth from different studies highlights new information brought by the KOKKY profile.

6. Discussion

The KOKKY seismic profile begins at 63.90° N, 22.95° E in Bothnian belt and ends at 60.61° N, 29.25° E near the eastern edge of Wiborg batholith. The use of a large number of portable seismometers reduced the timing uncertainty and allowed us to reliably assign blasts to known explosion sites within the geographic limits of those sites. Even though the largest time residuals in individual phase picks were ca. 0.2 s, 25 out of 63 events fulfilled the condition that at 5–6 phases could be used with a standard error of mean being less than 50 ms. Results are in agreement with those obtained in FIRE project in western Finland, but they also provide new information on crustal structure in the central part of the country. In general, the CFGC area is characterized by high velocity lower crust (Fig. 9) as already pointed out by Korja et al. (1993).

Nikkilä et al. (2016) suggested that the high velocity lower crust is formed by both crustal

differentiation process after three granitic melting stages and by mafic underplating during the latest magmatic event. CFGC is represented by overall thicker crust (63 km) and a thicker (high velocity) lower crustal layer (18 km) compared to the supracrustal Bothnian and Häme belts on its margins with overall crustal thicknesses of 54 and 43 km and lower crustal layer thicknesses of 12 km and 4 km, respectively. The upper crust in the western part of CFGC features slightly higher velocities than in the east. This may support the previously suggested hypothesis of higher amount of mafic and supracrustal rocks on the northwestern flank of CFGC (Lahtinen et al. 2016). Korja et al. (1993) interpreted the thin lower crustal layer below the Wiborg batholith area (SA) to result from the up-doming of mantle during extensional event forming the bimodal rapakivi magmatism (~ 1.63 Ga), but some of it may associated with partial melting of lower crust at late orogenic stages (~ 1.83 Ga). BB has previously been suggested to represent supracrustal margins of a ~ 1.86 Ga metamorphic core complex (Suikkanen et al. 2014; Kotilainen et al. 2016a, b).

One of the most important results of this investigation is confirmation of the existence of high velocity lower crust (HVLC) with a thickness of up to 19 km and determination of its velocity. Velocities 7.35–7.4 km/s obtained for HVLC are only slightly different from those obtained on almost perpendicular profile SVEKA'81, 7.3–7.35 km/s (Grad and Luosto 1987), and similar values, 7.35–7.42 km/s on the reinterpreted common transect of SVEKA'91 &

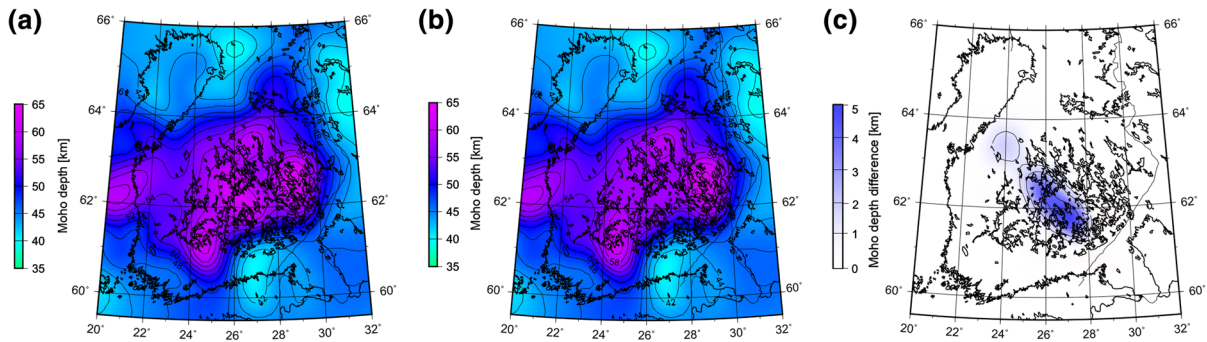


Figure 12

Moho depth maps of south-central Finland. **a** Map computed from data set of Grad et al. (2009) after adding Moho depth from the KOKKY ray tracing model into the original database. **b** Map after Grad et al. (2009) without new data. **c** Difference between the two Moho depth maps

SVEKA'81 profiles (Janik et al. 2007). When comparing these values, it should be noted that such discrepancies are within the method's accuracy limits. In this situation, it is also difficult to evaluate possible anisotropy. Another important research result is the extension of information about the region characterized by the deepest Moho in Europe, below CFGC.

Ray tracing analysis results from KOKKY profile can be conveniently added to the original dataset used to compute the European Moho depth map (Grad et al. 2009). The Moho depth in central and southern Finland extracted from Grad et al. (2009) was compared with new calculation with included data from the KOKKY profile, and difference of the resulting maps was also illustrated (Fig. 12). The KOKKY model provides new information at central part of the profile where Moho is 1–5 km deeper than known from previous reflection and refraction studies. The greatest difference is between old DSS profiles BALTIC (Luosto et al. 1990) and SVEKA81 (Luosto et al. 1984) which cross the KOKKY profile. However, on the reinterpreted common transect of SVEKA'91 and SVEKA'81 (Janik et al. 2007) the Moho depth seems to be similar. This result also replicates the observation of deepest Moho below CFGC around the city of Jyväskylä (Kozlovskaya et al. 2008) rather than below SA near the town of Heinävesi (Grad et al. 2009).

In Bouguer anomaly map of Finland, values increase gradually from Bothnian belt (BB) to Saimaa area (SA) and decrease from Saimaa area SA to Wiborg rapakivi batholith WRB along the line. Elo

(1997) found out that large granitoid batholiths, rapakivi granites in particular, are characterized by local gravity minima, while mafic rocks and exposures of middle crust are often associated with gravity maxima. Elo and Korja (1993) modeled that the Wiborg batholith is associated with a Bouguer anomaly minima surrounded by a maxima rising from the uplifted mantle. Central Finland granitoid complex is, however, not associated with a Bouguer minima, but rather appears to image side effects of minima associated with Bothnian belt and its granitic core and Wiborg rapakivi batholith. This supports the Kozlovskaya et al. (2004) idea that the CFGC is an upper crustal body, the crust below is thick and that Moho topography variations are compensated with thickness changes of the lower high-velocity lower crust and mafic intrusions within the upper parts.

Mass anomalies observed at surface, however, are generally compensated with mass distribution within the crust. It is not possible to solve a unique mass distribution from measured gravity values, but velocity data from seismic profiles are helpful in giving additional constraints for the Fennoscandian lithospheric structure. For example, Kuusisto et al. (2006) used mixtures of rock types with different V_p values to model crustal structure in the central part of shield, comparing data from FIRE1, FIRE3A, and SVEKA profiles. They found continuation of a bright reflector from FIRE1 to the nearby SVEKA profile, and the presence of three distinct layers and the transition from felsic to mafic lithology with depth also appeared evident in their results. The analysis of Finnish and Swedish earthquakes (Veikkolainen et al.

2017) resulted in the Fennoscandian seismic cut-off depth constraint 28 ± 4 km, which is also close to the boundary of upper and middle crust in Fig. 9.

7. Conclusions

The KOKKY profile crosses several other deep seismic sounding lines (FIRE1, SVEKA, and BALTIC). The line runs within less than 10 km distance from FIRE3A line, and these lines are parallel at a distance equivalent to 43% of entire length of KOKKY, 210 out of 490 km. This corresponds to FIRE3A common mid-points (CMPs) 12,000–18,000, an interval where the boundary of upper and middle crust dips at a greater depth in transition from Bothnian belt to CFGC. In FIRE3A, Moho can be clearly discerned only in the western end, corresponding to 40 km between CMPs 16,700–17,800. A strong reflector showing the boundary of upper and middle crust is visible in FIRE1 between line points 16,500–18,000, a section, which crosses KOKKY. The intersection of KOKKY and SVEKA is also close to this section, yet unlike in SVEKA, no shallow high velocity anomaly is visible in KOKKY. The Moho depth at the intersections of KOKKY line with reinterpreted common transect of SVEKA'91 and SVEKA'81 profiles (Janik et al. 2007) in CFGC, and with BALTIC profile, in SA (Janik 2010) seems to be similar. Comparison between earlier Moho depth map and the map updated with KOKKY results confirms clues about a depression in Moho boundary in central Finland, thus contributing to the interpretation of the SVEKALAPKO experiment (Kozlovskaya et al. 2008). The higher reflectivity of upper crust compared to middle and lower crust is most likely due to the actual crustal differentiation rather than a methodological bias (Kukkonen and Lahtinen 2006; Kuusisto et al. 2006). The uneven spatial distribution of shot points causes largest uncertainty to results in the boundary zone of BB and CFGC, where the distance between projected locations of shot points 12 and 13 is 78 km, and in eastern CFGC/western SA, where the distance between projected locations of shot points 26 and 27 is 103 km (Fig. 1, Table 2). Despite these deficiencies, the coverage of ray paths appears sufficient in all parts of

the profile (Figs. 6, 7, 8). The outcome of KOKKY is therefore encouraging for future plans to implement seismic profiling in similar manner in Finland and elsewhere, yet further analysis of accuracy and uncertainty of data in this kind of projects is also needed.

Acknowledgements

Open access funding provided by University of Helsinki including Helsinki University Central Hospital. This work was partially supported within statutory activities No 3841/E-41/S/2012-2019 of the Ministry of Science and Higher Education of Poland. Toni Veikkolainen received funding from Academy of Finland Grant 293449 to Annakaisa Korja within the framework of FIN-EPOS (Finnish Initiative of the European Plate Observing System). We appreciate the reviewers Alireza Malehmir and Marek Grad for their constructive criticism which helped us to improve the paper.

Open Access This article is licensed under a Creative Commons Attribution 4.0 International License, which permits use, sharing, adaptation, distribution and reproduction in any medium or format, as long as you give appropriate credit to the original author(s) and the source, provide a link to the Creative Commons licence, and indicate if changes were made. The images or other third party material in this article are included in the article's Creative Commons licence, unless indicated otherwise in a credit line to the material. If material is not included in the article's Creative Commons licence and your intended use is not permitted by statutory regulation or exceeds the permitted use, you will need to obtain permission directly from the copyright holder. To view a copy of this licence, visit <http://creativecommons.org/licenses/by/4.0/>.

Publisher's Note Springer Nature remains neutral with regard to jurisdictional claims in published maps and institutional affiliations.

REFERENCES

- BABEL Working Group. (1991). Evidence for early Proterozoic plate tectonics from seismic reflection profiles in the Baltic shield. *Nature*, 348, 34–38.
- Bogdanova, S. V. (1993). The three-segment hypothesis for the East European Craton. *Terra Nova*, 5, 313–314.

- Červený, V., & Pšenčík, I. (1984). Documentation of Earthquake Algorithms. In E. R. Engdahl (Ed.), *SEIS83—Numerical modeling of seismic wave fields in 2-D laterally varying layered structures by the ray method* (pp. 36–40). Boulder: Report SE-35.
- Elliott, B. A. (2003). Petrogenesis of the post-kinematic magmatism of the central Finland granitoid complex II; sources and magmatic evolution. *J Petrol*, *44*, 1681–1701.
- Elo, S. (1997). Interpretations of the gravity anomaly map of Finland. *Geophysica*, *33*, 51–80.
- Elo, S., & Korja, A. (1993). Geophysical interpretation of the crustal and the upper mantle structure in the Wiborg rapakivi granite area, southeastern Finland. *Precambrian Research*, *64*, 273–288.
- FENNIA Working Group. (1998). *P- and S-velocity structure of the Baltic Shield beneath the FENNIA profile in southern Finland*. Helsinki: Institute of Seismology, University of Helsinki, Report S-38.
- Grad, M., & Luosto, U. (1987). Seismic models of the crust of the Baltic Shield along the SVEKA profile in Finland. *Annales Geophysicae*, *5B*, 639–650.
- Grad, M., Tiira, T., & ESC Working Group. (2009). The Moho depth map of the European Plate. *Geophysical Journal International*, *176*, 279–292.
- Harju, S., Rämö, O. T., Mänttari, I., & Luttinen, A. V. (2010). The Taalikkala megaxenolith. In A. Heinonen, S. Lukkari, & O. T. Rämö (Eds.), *Guide to the IGCP-510 (A-type Granites and Related Rocks through Time) Field Trip Southeastern Finland, August 14–18, 2010* (pp. 22–25). Helsinki: Department of Geosciences and Geography.
- Havskov, J., & Ottemoller, L. (1999). SEISAN earthquake analysis software. *Seismological Research Letters*, *70*, 532–534.
- Heikkinen, P., & Luosto, U. (2000). Review of some features of the seismic velocity models in Finland. In: L. Pesonen, A. Korja, & S.-E. Hjelt (Eds.), *Lithosphere 2000. A symposium on the structure, composition and evolution of the lithosphere in Finland, October 4–5, 2000* (pp. 35–41). Espoo: Geological Survey of Finland, Extended Abstracts.
- Heinonen, A., Mänttari, I., Rämö, O. T., Andersen, T., & Larjamo, K. (2016). A priori evidence for zircon antecryst entrainment in megacrystic Proterozoic granites. *Geology*, *44*, 227–230.
- Heinonen, A. P., Rämö, O. T., Mänttari, I., Andersen, T., & Larjamo, K. (2017). Zircon as a proxy for the magmatic evolution of proterozoic Ferroan granites; the Wiborg Rapakivi Granite Batholith, SE Finland. *Journal of Petrology*, *58*, 2493–2517.
- Hobro, J. W., Singh, S. C., & Minshull, T. A. (2003). Three-dimensional tomographic inversion of combined reflection and refraction seismic traveltime data. *Geophysical Journal International*, *152*, 79–93.
- Höglttä, P., & Heilimo, E. (2017). Metamorphic Map of Finland. In M. Nironen (Ed.), *Bedrock of Finland at the scale 1: 1,000,000—major stratigraphic units, metamorphism and tectonic evolution*, *Geological Survey of Finland, Special Paper*, *60* (pp. 75–126). Espoo: Geological Survey of Finland.
- Hyyönen, T., Tiira, T., Korja, A., Heikkinen, P., Rautioaho, E., & SVEKALAPKO Seismic Tomography Working Group. (2007). A tomographic crustal velocity model of the central Fennoscandian shield. *Geophysical Journal International*, *168*, 1210–1226.
- Janik, T. (2010). Upper lithospheric structure in the central Fennoscandian shield: Constraints from P- and S-wave velocity models and V_p/V_s ratio distribution of the BALTIC wide-angle seismic profile. *Acta Geophysica*, *58*, 543–586.
- Janik, T., Kozlovskaya, E., & Yliniemi, J. (2007). Crust-mantle boundary in the central Fennoscandian shield: Constraints from wide-angle P and S wave velocity models and new results of reflection profiling in Finland. *Journal of Geophysical Research*, *112*, B04302. <https://doi.org/10.1029/2006JB004681>.
- Kähkönen, Y. (2005). Svecofennian supracrustal rocks. In M. Lehtinen, P. A. Nurmi, & O. T. Rämö (Eds.), *Precambrian geology of Finland—key to the evolution of the Fennoscandian shield* (pp. 343–406). Amsterdam: Elsevier.
- Komminaho, K., (1998). Software manual for programs MODEL and XRAYS: A graphical interface for SEIS83 program package. Oulu: University of Oulu, Department of Geophysics, Report 20.
- Korja, A., & Heikkinen, P. J. (2008). Seismic images of Paleoproterozoic microplate boundaries in the Fennoscandian shield. *Geological Society of America Special Paper*, *440*, 229–248.
- Korja, A., Korja, T., Luosto, U., & Heikkinen, P. (1993). Seismic and geoelectric evidence for collisional and extensional events in the Fennoscandian Shield—implications for Precambrian crustal evolution. *Tectonophysics*, *219*, 129–152.
- Kotilainen, A. K., Mänttari, I., Kurhila, M., Höglttä, P., & Rämö, O. T. (2016a). Evolution of a Palaeoproterozoic giant magmatic dome in the Finnish Svecofennian; new insights from U–Pb geochronology. *Precambrian Research*, *272*, 39–56.
- Kotilainen, A. K., Mänttari, I., Kurhila, M., Höglttä, P., & Rämö, O. T. (2016b). New monazite U–Pb age constraints on the evolution of the Paleoproterozoic Vaasa granitoid batholith, western Finland. *Bulletin of the Geological Society of Finland*, *88*, 5–20.
- Kozlovskaya, E., Elo, S., Hjelt, S.-E., Yliniemi, J., Pirttijärvi, M., & SVEKALAPKO Seismic Tomography Working Group. (2004). 3-D density model of the crust of southern and central Finland obtained from joint interpretation of the SVEKALAPKO crustal P-Wave velocity models and gravity data. *Geophysical Journal International*, *158*, 827–848.
- Kozlovskaya, E., Kosarev, G., Aleshin, I., Riznichenko, O., & Sanina, I. (2008). Structure and composition of the crust and upper mantle of the Archean-Proterozoic boundary in the Fennoscandian shield obtained by joint inversion of receiver function and surface wave phase velocity of recording of the SVEKALAPKO array. *Geophysical Journal International*, *175*, 135–152.
- Kukkonen, I. T., & Lahtinen, R. (Eds.). (2006). *Finnish reflection experiment FIRE 2001–2005. Geological Survey of Finland, Special Paper* (p. 247). Espoo: Geological Survey of Finland.
- Kuusisto, M., Kukkonen, I. T., Heikkinen, P., & Pesonen, L. J. (2006). Lithological interpretation of crustal composition in the Fennoscandian Shield with seismic velocity data. *Tectonophysics*, *420*, 283–299.
- Lahtinen, R., Huhma, H., Kontinen, A., Kohonen, J., & Sorjonen-Ward, P. (2010). New constraints for the source characteristics, deposition and age of the 2.1–1.9 Ga metasedimentary cover at the western margin of the Karelian Province. *Precambrian Research*, *176*, 77–93.
- Lahtinen, R., Huhma, H., Lahaye, Y., Lode, S., Heinonen, S., Sayab, M., et al. (2016). Paleoproterozoic magmatism across the Archean-Proterozoic boundary in central Fennoscandia: Geochronology, geochemistry and isotopic data (Sm–Nd, Lu–Hf, O). *Lithos*, *262*, 507–525.

- Lahtinen, R., Korja, A., Nironen, M., & Heikkinen, P. (2009). Palaeoproterozoic accretionary processes in Fennoscandia. *Geological Society Special Publications*, 318, 237–256.
- Luosto, U. (1984). Recent DSS profiles in Finland. In D. A. Galson & S. Mueller (Eds.), *Proceedings of the first workshop on the European Geotraverse (EGT), the northern segment* (pp. 105–108). Einsiedeln: European Science Foundation.
- Luosto, U. (1997). Structure of the Earth's crust in Fennoscandia as revealed from refraction and wide-angle reflection studies. *Geophysica*, 33, 3–16.
- Luosto, U., Grad, M., Guterch, A., Heikkinen, P., Janik, T., Komminaho, K., et al. (1994). Crustal structure along the SVEKA 91 profile in Finland. In K. Makropoulos & P. Suhadolc (Eds.), *European Seismological Commission. XXIV General Assembly, Proceedings and Activity Report 1992–1994* (Vol. II, pp. 974–983). Athens: European Seismological Commission.
- Luosto, U., Lanne, E., Korhonen, H., Guterch, A., Grad, M., Materzok, R., et al. (1984). Deep structure of the Earth's crust on the SVEKA profile in central Finland. *Annales Geophysicae*, 2, 559–570.
- Luosto, U., Tiira, T., Korhonen, H., Azbel, I., Burmin, V., Buyanov, A., et al. (1990). Crust and upper mantle structure along the DSS Baltic profile in SE Finland. *Geophysical Journal International*, 101, 89–110.
- Mäkitie, H., Kärkkäinen, N., Lahti, S. I., & Lehtonen, M. I. (1999). Chemical and modal composition of granitoids in three different geological units, South Pohjanmaa, western Finland. *Geological Survey of Finland Special Paper*, 27, 7–19.
- Malinowski, M. (2013). Models of the Earth's crust from controlled-source seismology—where we stand and where we go? *Acta Geophysica*, 61, 1437–1456.
- McCaughy, M., & Singh, S. (1997). Simultaneous velocity and interface tomography of normal-incidence and wide-aperture seismic traveltimes data. *Geophysical Journal International*, 131, 87–99.
- Nikkilä, K., Korja, A., Koyi, H., & Eklund, O. (2015). Analog modeling of one-way gravitational spreading of hot orogens—A case study from the Svecofennian orogeny, Fennoscandian Shield. *Precambrian Research*, 268, 135–152.
- Nikkilä, K., Mänttari, I., Nironen, M., Eklund, O., & Korja, A. (2016). Three stages to form a large batholith after terrane accretion—an example from the Svecofennian orogen. *Precambrian Research*, 281, 618–638.
- Nironen, M. (2017). *Bedrock of Finland at the scale 1:1,000,000—Major stratigraphic units, metamorphism and tectonic evolution. Geological Survey of Finland, Special Paper* (Vol. 60, p. 128). Espoo: Geological Survey of Finland.
- Ollikainen, M., & Ollikainen, M. (2004). *The Finnish Coordinate Reference Systems* (p. 17). Kirkkonummi: Finnish Geodetic Institute.
- Press, W. H., Teukolsky, S. A., Vetterling, W. T., & Flannery, B. P. (1992). *Numerical recipes in FORTRAN: The art of scientific computing* (2nd ed.). New York: Cambridge University Press.
- Rämö, O. T., & Haapala, I. (2005). Rapakivi granites. In M. Lehtinen, P. A. Nurmi, & O. T. Rämö (Eds.), *Precambrian geology of Finland—key to the evolution of the Fennoscandian Shield* (pp. 533–562). Amsterdam: Elsevier.
- Sorjonen-Ward, P. (2006). Geological and structural framework and preliminary interpretation of the FIRE 3 and FIRE 3A reflection seismic profiles. In I. Kukkonen & R. Lahtinen (Eds.), *Finnish Reflection Experiment 2001–2005, Geological Survey of Finland, Special Paper* (Vol. 43, pp. 105–159). Espoo: Geological Survey of Finland.
- Spada, M., Bianchi, I., Kissling, E., Piana Agostinetti, N., & Wiemer, S. (2013). Combining controlled-source seismology and receiver function information to derive 3-D Moho topography for Italy. *Geophysical Journal International*, 194, 1050–1068.
- Suikkanen, E., Huhma, H., Kurhila, M., & Lahaye, Y. (2014). The age and origin of the Vaasa migmatite complex revisited. *Bulletin of the Geological Society of Finland*, 86, 41–55.
- Tiira, T., Janik, T., Kozlovskaya, E., Grad, M., Korja, A., Komminaho, K., et al. (2013). Crustal Architecture of the Inverted Central Lapland Rift Along the HUKKA 2007 Profile. *Pure and Applied Geophysics*, 171, 1129–1152.
- Veikkolainen, T., Kukkonen, I. T., & Tiira, T. (2017). Heat flow, seismic cut-off depth and thermal modeling of the Fennoscandian Shield. *Geophysical Journal International*, 211, 1414–1427.
- Vorma, A. (1975). On two roof pendants in the Wiborg rapakivi massif, southeastern Finland. *Geological Survey of Finland, Bulletin*, 272, 86.
- Zelt, C. A. (1994). *ZPLOT—an interactive plotting and picking program for seismic data*. Cambridge: Bullard Laboratory, University of Cambridge.